The Effect of Stent Implantation on the Deformations of the SFA and the Popliteal Artery: In-Vivo 3D Deformational Analysis from 2D Radiographs

Abstract

The objective of this work was to develop a system for 3D reconstruction of the femoro-popliteal artery from two angiographic views and to quantify the in-vivo 3D deformations of 18 patients prior to balloon angioplasty and following primary stent implantation. The procedure had an insignificant effect on the bending behavior of the artery, as the average mean curvature change remained constant before (0.04 ± 0.03 cm^{-1}) and after stent implantation (0.03 ± 0.04 cm^{-1}) within the lesion. A significant effect of stent implantation was measured in terms of a decrease in arterial shortening during leg flexion.

1. Introduction

Stent fractures have been frequently associated with arterial deformations [1, 2], but the effect of fractured struts on in-stent restenosis is contradictory [3, 4]. Even though, improved stent design has significantly decreased the occurrence of stent failures, changes in the mechanical environment distal or proximal to the stented arterial segment, could lead to arterial kinking and chronic trauma. This effect might be one explanation for the high restenosis rates observed in the femoro-popliteal (FP) arteries [5].

Quantification of the arterial deformations following primary stent implantation is required to understand the relationship between the mechanical environment and high restenosis rates observed in the stented FP artery. Several groups have proposed methods to assess the dynamic conformational changes of the artery during leg movement [6-9]. With the exception of one, these studies fail to characterize the arterial deformations on stented arteries in-vivo and none describe the deformations of bare arteries in close vicinity of the stented segments.

Therefore, the objective of this study was to estimate the in-vivo deformational changes of the FP artery before balloon angioplasty and after primary stent implantation. Two angiographic images of the leg in straight and flexed positions were used to determine a 3D representation of the arterial tree. The resulting 3D patient-specific representations were subsequently aligned and the changes in length and curvature were measured.

2. Materials and Methods

Ethical approval

Institutional Review Board approval for this study was obtained by the *BLINDED*. The present study was performed in accordance to the Declaration of Helsinki and informed consent was obtained from all individual participants.

Angiography

18 patients (12 males; mean age: 68 ± 8.6) scheduled for PAD treatment were recruited for this study. A series of angiographic images were acquired as part of the normal clinical routine. Prior to balloon angioplasty and following primary stent implantation, angiographic images were acquired with a Philips Allura FD 20 Xper X-ray system with Clarity Upgrade (Best, Netherlands) and recurrent injection of contrast agent. During the intervention, the balloon was inflated to approximately 10 atmospheres. Following balloon angioplasty of the arterial calcifications, 15 patients underwent placement of one self-expanding Nitinol stent, whereas 3 patients received two stents (Table 1). The lengths and types of the stents were selected by the operator based on the lengths, morphologies and locations of the lesions. The patients were adjusted in supine position, and angiographic images of the straight and flexed leg (hip/knee flexion of 20°/70°) were obtained. The acquired images were stored on the workstation in terms of subtraction angiography and cine-images. In order to determine the spatial relationship between the angiographic images, a small-sized calibration object was conveniently attached to the patient's thigh using a strap [10].

3D model reconstruction

The 3D reconstruction of the arterial tree relies on a pair of angiographic images, which were interactively selected out of the series of images, having a view angle larger than 25°. For each image the 2D boundaries of the main branch were semi-automatically outlined using live-wire algorithm [11]. In addition, points along the centerlines of a certain number of side-branches were interactively picked (s. Fig. 1). The extraction of corresponding sections is thereby guided by the visualization of epipolar lines [12]. The uniformly interpolated boundaries of the main branch together with the particular calibration information are then used to perform a straightforward multi-view reconstruction as for example described by Movassaghi et al. [13]. The side-branches were reconstructed in the same way. As only centerline points were defined for the side-branches, the particular points were directly triangulated. A surface model of a reconstructed arterial tree is shown in Figure 1.

Reconstruction Analysis

To analyze the multi-view reconstruction capability, the forward- and backward projection accuracy of the arterial tree was assessed with respect to an additional validation view. This validation view was also interactively selected, whereas the view direction had to be different (at least 20° apart) than the two views used for 3D reconstruction. The forward projection error results out of the average error distance between the projected points (from the reconstructed model) and the extracted boundary information (defined in the validation view). The backward-projection error is determined by computing epipolar lines for each 2D centerline point (of main branch and side-branches) of the validation view and computing the distance to the closest vertex of the reconstructed model.

Deformation Analysis

The deformation of the FP artery was quantified by measuring its axial elongation and its curvature. The elongation ε was determined as the ratio of the total change in arterial length Δl and the initial length in straight position $l_{straight}$:

$$\varepsilon = \frac{\Delta l}{l_0} = \frac{l_{flexed} - l_{straight}}{l_{straight}} \cdot 100\%$$

The arterial length *l* was thereby measured as the distance along the main arterial centerline between corresponding side-branches. The curvature was assessed by successively fitting a circle to triplets of centerline points [14]. Accordingly, the curvature is defined as the inverse of the circle radius. This fitting process was performed along the entire centerline (sampling spacing of 1.25 mm) and the mean and maximum curvature values were subsequently determined for each reconstructed artery. Paired t-tests were used to evaluate the changes in arterial lengths and curvatures due to leg flexion and stent implantation.

3. Results

For each of the 18 patients, four angiographic datasets (pre- and post-angioplasty in straight and flexed position) were analyzed. For one patient (patient 2), the artery reconstruction was not possible in the pre-angioplasty stage as the main branch was only partially visible due to severe arterial calcification. 19 datasets were available for assessing the reconstruction accuracy. The average angle between a pair of views used for 3D reconstruction was 37.9 ± 8.0° and between the validation view and its closest view used for reconstruction was 28.5 ± 9.1°. The forward projection error was 1.18 ± 0.28 mm on average (max. error: 1.44 mm) and the average backward reconstruction error was 1.03 ± 0.15 mm (max. error: 1.24 mm).

On average, the popliteal artery had the largest maximum curvature change (pre-angioplasty: 0.29 ± 0.14; post-stent: 0.34 ± 0.16; *P*: 0.04), followed by the distal-SFA (pre-angioplasty: 0.13 ± 0.05; post-stent: 0.16 ± 0.16; *P*: 0.04) and the mid-SFA (pre-angioplasty: 0.09 ± 0.03; post-stent: 0.12 ± 0.11; *P*: 0.02). A slight decrease in average arterial shortening was found after angioplasty (s. Table 2). The difference is larger within the lesions, where the stent implantation has induced a statistically significant lower shortening during flexion compared to the diseased states of the arteries (*P*: 0.01). Arterial shortening also differed between stent types, with Zilver PTX showing less shortening after stent implantation compared to the Everflex and Pulsar stents. No difference was found in the overall bending behavior before angioplasty and after stent implantation. However, seven patients showed arterial kinking after the procedure. For six of the patients, this extreme deformation occurred in the popliteal artery, adjacent to the distal end of the stents. In the remaining case, the kinking was observed in the distal SFA and adjacent to the proximal end of the stent (adjacency refers to a margin of 1 cm).

4. Discussion

The effects of the mechanical environment created due to leg flexion on in-stent restenosis in the FP arteries are not clear. To this end, a method for the 3D artery reconstruction has been developed and validated. The reported reconstruction errors correspond well with data published in literature. Based on 4-5 projections of the coronary artery, Liao et al. [15] reported a mean back-projection error of 1.18 mm. The RMS forward projection error of the FP arterial centerline was reported by Klein et al. [9] to be 2.13 mm for the leg in straight position and 1.61 mm for the leg in flexed position. For both diseased and treated arteries, the deformations of the regions in close proximity to the knee are increasingly affected by leg flexion. The effect of stent implantation on the overall stiffness of the arterial segment indicates that the procedure decreases axial elongation, but doesn't affect the average arterial curvature. However, arterial kinking occurs when the stents are placed in the vicinity of arterial segments that are subject to heavy mechanical loads such as the distal SFA or popliteal segment artery. The same behavior was observed for all types of stents, indicating that large arterial deformation is primarily associated with stent positioning along the arterial tract. A possible reason for this kinking deformation is the axial stiffening introduced by the stent, which limits the possible displacement of the flexible segment of the artery during flexion of the leg. A similar behavior was also observed for severe calcifications prior to stent implantation, where large arterial curvatures were measured in the distal SFA/popliteal segments. These maximum localized curvatures in the bare arteries adjacent to the stents may trigger re-occlusion and restenosis.

Even though these characteristics were observed for all considered patient datasets, they need to be further confirmed by follow-on studies. Due to the sample size, only a basic statistical analysis could be conducted. Another limitation of this study is the 3D reconstruction from only two views. As the arterial tree is reasonably complex, an adequate reconstruction of overlapping structures is restricted. Moreover, 3D reconstructions from a limited number of views commonly suffer from foreshortening effects.

In conclusion, a better understanding of the mechanical environment of the FP artery is necessary to improve the clinical treatment and thus to reduce the restenosis rate. Even though further clinical trials need to be conducted, the feasibility of using 2D/3D reconstruction to assess the in vivo deformational characteristics of the artery before and after angioplasty could be demonstrated.

Conflict of interest statement

The authors have no conflict of interest related to this work.

References

[1] Rits J, van Herwaarden JA, Jahrome AK, Krievins D. Moll FL (2008) The incidence of arterial stent fractures with exclusion of coronary, aortic and non-arterial settings. Eur J Vasc Endovasc Surg 36(3):339-45.

[2] Adlakha S, Sheikh M, Wu J, Burket MW, Pandya U, Colyer W, Eltahawy E, Cooper CJ (2010) Stent fracture in the coronary and peripheral arteries. J Interv Cardiol 23(4):411-9.

[3] Windecker S, Remondino A, Eberli FR, Jüni P, Räber L, Wenaweser P, Togni M, Billinger M, Tüller D, Seiler C, Roffi M, Sütsch G, Maier W, Lüscher T, Hess OM, Egger M, Meier B (2005) Sirolimus-eluting and paclitaxel-eluting stents for coronary revascularization. N Engl J Med 353(7):653-62.

[4] Bosiers M, Torsello G, Gissler HM, Ruef J, Müller-Hülsbeck S, Jahnke T, Peeters P, Daenens K, Lammer J, Schoe H, Mathias K, Koppensteiner R, Vermassen F, Scheinert D (2009) Nitinol Stent Implantation in Long Superficial Femoral Artery Lesions: 12-Month Results of the DURABILITY I Study. Journal Endovasc Ther 16(3): 261-9.

[5] Arena FJ (2005) Arterial kink and damage in normal segments of the superficial femoral and popliteal arteries abutting nitinol stents – a common cause of late occlusion and restenosis? A single-center experience. J Invasive Cardiol 17(9):482-6.

[6] Klein AJ, Chen SJ, Messenger JC, Hansgen AR, Plomondon ME, Carroll JD, Casserly IP (2009) Quantitative assessment of the conformational change in the

femoropopliteal artery with leg movement. Catheter Cardiovasc Interv 74(5):787-98.

[7] Cheng CP, Wilson NM, Hallett RL, Herfkens RJ, Taylor CA (2006) In vivo MR angiographic quantification of axial and twisting deformations of the superficial femoral artery resulting from maximum hip and knee flexion. J Vasc Interv Radiol 17(6):979-87.

[8] Gökgöl C, Diehm N, Kara L, Büchler P. (2013) Quantification of popliteal artery deformation during leg flexion in subjects with peripheral artery disease: a pilot study. J Endovasc Ther 20(6):828-35.

[9] Klein AJ, Casserly IP, Messenger JC, Carroll JD, Chen SY (2009) In vivo 3D modeling of the femoropopliteal artery in human subjects based on x-ray angiograph: methodology and validation. Medical Physics 36(2):289-310.

[10] Schumann S, Dong X, Puls M, Nolte LP, Zheng G (2012) Calibration of c-arm for orthopaedic interventions via statistical model-based distortion correction and robust phantom detection. The International Symposium on Biomedical Imaging: From Nano to Macro (ISBI):1204-7.

[11] Barrett WA, Mortensen EN (1997) Interactive live-wire boundary extraction. Med Image Anal 1(4):331–41.

[12] Hartley R, Zisserman A (2004) Multiple view geometry in computer vision. 2nd ed. Cambridge: Cambridge University Press

[13] Movassaghi B, Rasche V, Grass M, Viergever MA, Niessen WJ (2004) A quantitative analysis of 3-D coronary modeling from two or more projection images. IEEE Trans Med Imaging 23(12):1517-31.

[14] Choi G, Cheng CP, Wilson NM, Taylor CA (2009) Methods for quantifying three-dimensional deformation of arteries due to pulsatile and nonpulsatile forces: Implications for the design of stents and stent grafts. Ann Biomed Eng 37(1):14-33.

[15] Liao R, Luc D, Sun Y, Kirchberg K (2010) 3-D reconstruction of the coronary artery tree from multiple views of a rotational x-ray angiography. Int J Cardiovasc Imaging 26(7):733-49.

Tables

patient no.	age	gender	calcification level	lesion		implanted stents*	
				location	length	Type	Size
1	65	M	Moderate	Mid SFA/ Distal SFA	60 mm	Pulsar 18	Ø6 x 40 mm
2	75	M	Moderate	Distal SFA / Popliteal	180 mm	Pulsar 18	Ø6 x 200 mm
3	56	M	Moderate	Mid SFA/ Distal SFA	50 mm	Xpert	Ø4 x 40 mm
4	68	F	Moderate	Mid SFA	60 mm	Zilver PTX	Ø5 x 80 mm
5	66	F	In-stent re-occlusion	Prox. SFA / Mid SFA	200 mm	EverFlex	Ø5 x 150 mm
6	75	M	Severe	Mid SFA / Distal SFA	180 mm	EverFlex	Ø6 x 200 mm
7	79	F	Severe	Prox. SFA / Distal SFA	350 mm	Pulsar-18 (x2)	Ø5 x 200 mm
8	71	M	Severe	CFA** / Distal SFA	350 mm	EverFlex (x2)	Ø6 x 200 mm
9	66	F	Moderate	Prox. SFA / Distal SFA	300 mm	Pulsar-18	Ø5 x 200 mm
10	76	F	Severe	Prox. SFA / Distal SFA	400 mm	Everflex (x2)	Ø6 x 200 mm
11	65	M	Moderate	Distal SFA	100 mm	Zilver PTX	Ø6 x 120 mm
12	71	M	Moderate	Mid SFA / Distal SFA	100 mm	Zilver PTX	Ø6 x 120 mm
13	81	M	Moderate	Popliteal	70 mm	Pulsar-18	Ø5 x 80 mm
14	48	M	Severe	Mid SFA / Distal SFA	50 mm	Everflex	Ø6 x 60 mm
15	79	F	Severe	Mid SFA	80 mm	Everflex	Ø5 x 100 mm
16	61	M	Moderate	Mid SFA	100 mm	Zilver PTX	Ø5 x 120 mm
17	62	M	Moderate	Prox. SFA / Mid SFA	300 mm	Everflex	Ø6 x 200 mm
18	65	M	Moderate	Distal SFA	100 mm	Zilver PTX	Ø6 x 120 mm

Table 1: Patient demographics, level of calcification, as well as the description of the lesions and implanted stents.

*Pulsar 18: Biotronik AG, Bülach Switzerland; Xpert: Abbott Vascular, Santa Clara, CA, USA; Zilver PTX: Cook Medical Inc., Bloomington, IN, USA; EverFlex: Ev3 Endovascular Inc., Plymouth, MN, USA

	axial elongation (%)	curvature change (cm^{-1})	
		mean	**max**
Pre-Angio			
Proximal to lesion	-8.0	0.11	0.28
Lesion	-6.4 ± 3.4	0.04 ± 0.03	0.12 ± 0.04
Distal to lesion	-12.8 ± 3.6	0.10 ± 0.06	0.28 ± 0.14
Post-Stent			
Proximal to lesion	-8.7 ± 8.7	0.08 ± 0.10	0.18 ± 0.19
Lesion	-3.2 ± 2.9	0.03 ± 0.04	0.16 ± 0.14
Distal to lesion	-9.3 ± 6.7	0.09 ± 0.07	0.24 ± 0.18
Pulsar-18			
Proximal to stent	-10.3 ± 13.8	0.10 ± 0.11	0.30 ± 0.31
Stent	-4.6 ± 3.6	0.04 ± 0.04	0.22 ± 0.21
Distal to stent	-13.2 ± 14.2	0.09 ± 0.09	0.20 ± 0.07
Everflex			
Proximal to stent	-5.2 ± 1.4	0.01 ± 0.01	0.08 ± 0.03
Stent	-3.2 ± 2.7	0.03 ± 0.03	0.14 ± 0.08
Distal to stent	-9.5 ± 5.3	0.11 ± 0.08	0.33 ± 0.21
Zilver-PTX			
Proximal to stent	-14.6 ± 10.0	0.14 ± 0.17	0.22 ± 0.23
Stent	-1.62 ± 2.3	0.04 ± 0.06	0.15 ± 0.18
Distal to stent	-8.8 ± 6.4	0.08 ± 0.07	0.21 ± 0.14

Table 2: Overview of the average change in the axial elongation and curvature values of 18 patients due to leg flexion measured before balloon angioplasty (pre-angio) and after primary stent implantation (post-stent) within the lesion and regions that are proximal or distal to the lesions. Differences between the deformations measured for three different stent types are also reported.

Figures

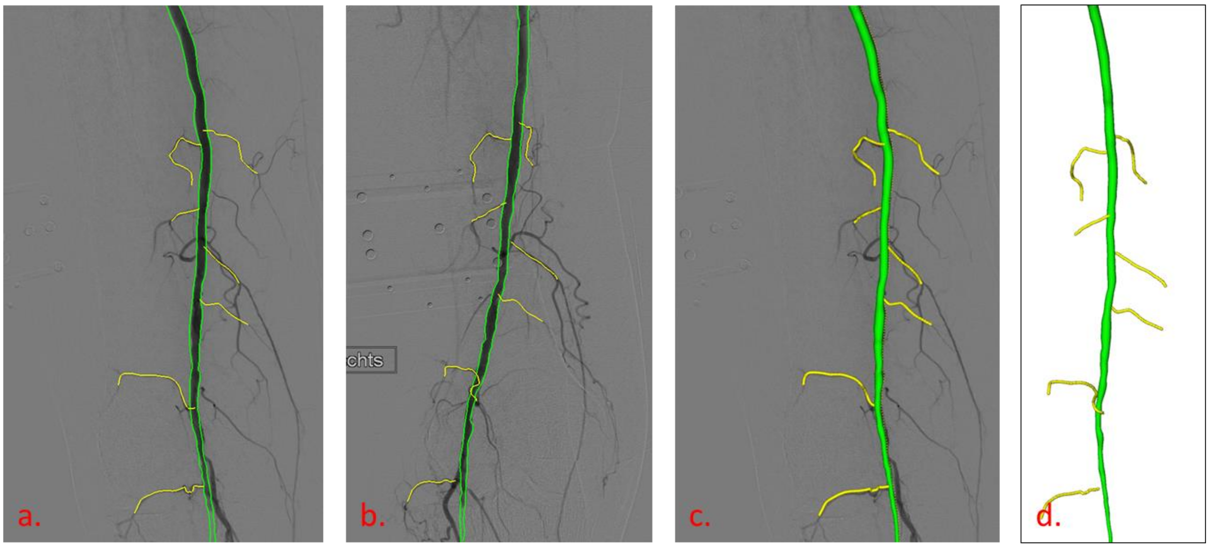

Fig. 1: a, b: Pair of angiographic images with semi-automatically extracted arterial tree; c: Reconstructed arterial tree on top of radiograph; d: Reconstructed arterial tree

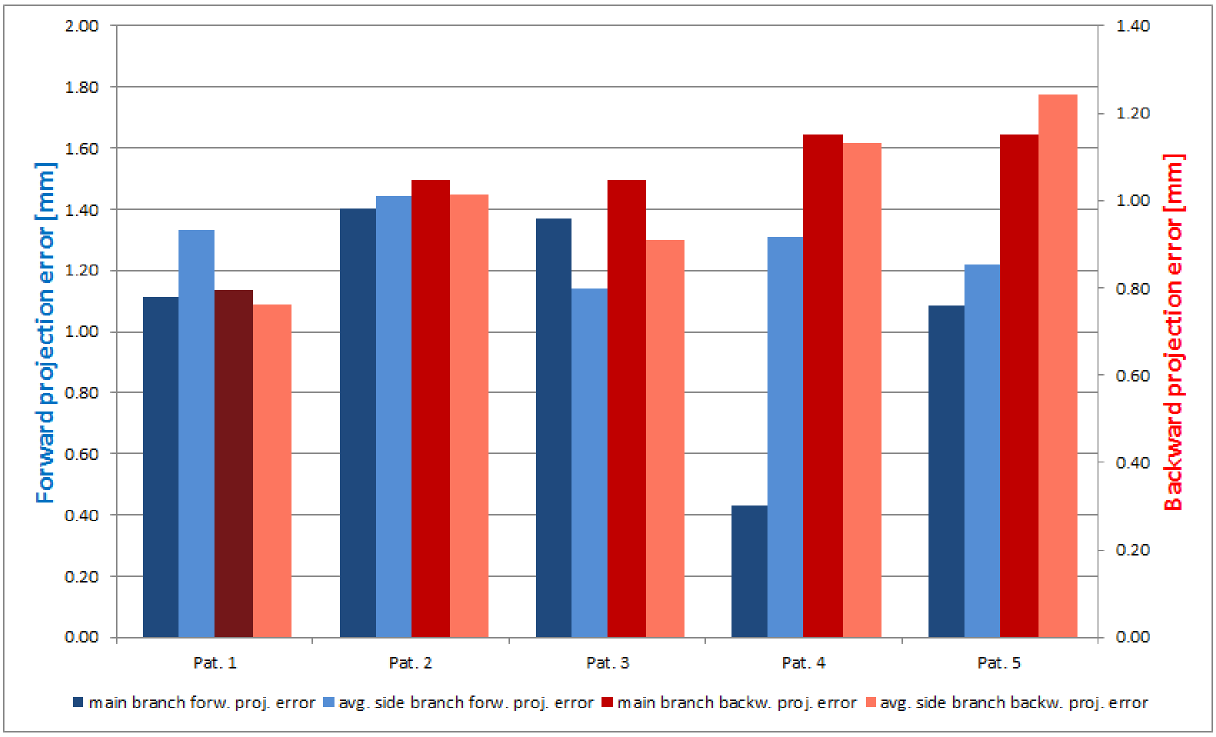

Fig. 2: Error plot of forward (left two columns of each patient) and backward projection error (right two columns of each patient).